Vol. 92 No. 4 pp. 1334–1348 ACTA GEOLOGICA SINICA (English Edition) Aug. 2018

Latest Triassic to Early Jurassic Thrusting and Exhumation in the Southern Ordos Basin, North China: Evidence from LA-ICP-MS-based Apatite Fission Track Thermochronology

ZHANG Shaohua[1], LIU Chiyang[1], YANG Minghui[2], BAI Jianke[1, 3] and WANG Jianqiang[1, *]

1 *State Key Laboratory of Continental Dynamics, Department of Geology, Northwest University, Xi'an 710069, China*

2 *State Key Laboratory of Petroleum Resource and Prospecting, College of Geosciences, China University of Petroleum, Beijing 102200, China*

3 *Research Center of Orogenic Geology, Xi'an Center of Geological Survey, China Geological Survey, Xi'an 710054, China*

Abstract: The contractional structures in the southern Ordos Basin recorded critical evidence for the interaction between Ordos Basin and Qinling Orogenic Collage. In this study, we performed apatite fission track (AFT) thermochronology to unravel the timing of thrusting and exhumation for the Laolongshan-Shengrenqiao Fault (LSF) in the southern Ordos Basin. The AFT ages from opposite sides of the LSF reveal a significant latest Triassic to Early Jurassic time-temperature discontinuity across this structure. Thermal modeling reveals at the latest Triassic to Early Jurassic, a ~50°C difference in temperature between opposite sides of the LSF currently exposed at the surface. This discontinuity is best interpreted by an episode of thrusting and exhumation of the LSF with ~1.7 km of net vertical displacement during the latest Triassic to Early Jurassic. These results, when combined with earlier thermochronological studies, stratigraphic contact relationship and tectono-sedimentary evolution, suggest that the southern Ordos Basin experienced coeval intense tectonic contraction and developed a north-vergent fold-and-thrust belt. Moreover, the southern Ordos Basin experienced a multi-stage differential exhumation during Mesozoic, including the latest Triassic to Early Jurassic and Late Jurassic to earliest Cretaceous thrust-driven exhumation as well as the Late Cretaceous overall exhumation. Specifically, the two thrust-driven exhumation events were related to tectonic stress propagation derived from the latest Triassic to Early Jurassic continued compression from Qinling Orogenic Collage and the Late Jurassic to earliest Cretaceous intracontinental orogeny of Qinling Orogenic Collage, respectively. By contrast, the Late Cretaceous overall exhumation event was related to the collision of an exotic terrain with the eastern margin of continental China at ~100 Ma.

Key words: fission track thermochronology, thermal history modeling, thrusting and exhumation, Ordos Basin, Qinling Orogenic Collage

1 Introduction

The process of tectonic stress propagation from the orogen to the adjacent stable plates is well known and has been applied to interpret the deformation and evolution of the transition zones between orogen and adjacent stable plates (Holford et al., 2009; Li et al., 2010; Merten et al., 2011; Tian et al., 2012; Gautheron et al., 2013; Savignano et al., 2016; Zhao Xiaochen et al., 2016; Bande et al., 2017; Yang et al., 2017; Zhang Beihang et al., 2017). Therefore, the original deformation characteristics of the transition zones provide critical evidence for the interaction between orogen and adjacent stable plates through time and space (Witt et al., 2012; Dielforder et al., 2016). Unfortunately, the original deformation records of the transition zones are not always completely preserved due to the later tectonic superposition and/or erosion (Giorgis et al., 2017). This makes it is challenging to thoroughly unravel the interaction between orogen and

* Corresponding author. E-mail: wjq@nwu.edu.cn

adjacent stable plates.

From the perspective of tectonic geomorphology, the Mesozoic Ordos Basin is separated from the Qinling Orogenic Collage by the Cenozoic Weihe Graben to the south (Du Jianjun et al., 2017; Meng Qingren, 2017). Therefore, most of original deformation records regarding the pre-Cenozoic interaction between the Qinling Orogenic Collage and Ordos Basin have been deeply buried beneath the Weihe Graben by Cenozoic intense subsidence. Fortunately, the southern Ordos Basin seems to preserve some pre-Cenozoic deformation records mostly as contractional structures, e.g. thrust fault and fold, although some studies argued the exhumation of the southern Ordos Basin was mainly caused by the tilting of rift shoulder related to the evolution of Cenozoic Weihe Graben (Wang Jianqiang et al., 2015). In addition, other studies (Chen Gang and Zhou Dingwu, 1994; Zhou Dingwu et al., 2002) have linked these contractional structures to the Middle Paleozoic collision of the North China Plate and the South Qinling along the Shangdan Suture (Meng and Zhang, 1999, 2000) or to the Late Jurassic to Early Cretaceous intracontinental orogeny due to the southward intracontinental subduction of the North China Plate beneath the Qinling Orogenic Collage and continuously northward subduction of the South China Plate (Dong et al., 2016). Obviously, the timing of deformation of these contractional structures is still amphibolous and hampers efforts to better understand the interaction between the Qinling Orogenic Collage and Ordos Basin.

Determination of timing of crustal deformation is always challenging, especially when deformation-related strata are poorly preserved (Duvall et al., 2011). Low-temperature thermochronology, including $^{3}He/^{4}He$, (U-Th)/He, fission track, and $^{40}Ar/^{39}Ar$ thermochronology, has emerged as a useful method based on the thermal effect of crustal deformation (Ehlers et al., 2001; Tagami, 2005, 2012; Zheng et al., 2006; Gautheron et al., 2013; Wang et al., 2014; Maino et al., 2015; Giorgis et al., 2017; Sueoka et al., 2017). Apatite fission track thermochronology has been proven to be an effective tool for dating rock exhumation that accompany fault activity (West and Roden-Tice, 2003; Fitzgerald et al., 2009; Ring and Bernet, 2010; Blythe and Longinotti, 2013; Tremblay et al., 2013). For most apatite samples, fission tracks are fully retained at temperature below 60°C, whereas they are only partially retained between 60°C and 120°C (apatite partial annealing zone, APAZ) with a mean closure temperature of 110°(±10)°C (Gleadow et al., 1983; Green et al., 1989). If no apparent displacement has occurred across the fault zone, then the AFT ages should be zero for the same buried depth in both the foot-wall and hanging-wall samples buried below the APAZ. However, if the foot-wall and/or the hanging-wall rocks exhumed the closure temperature due to fault activity, then the AFT thermometer will work and record the timing for faulting (Zheng et al., 2006; Tremblay et al., 2013; Cheng Xiaogan et al., 2016).

Although several AFT thermochronological studies have been applied to the southern Ordos Basin during the last decade (Chen Gang et al., 2007; Wang Jianqiang et al., 2010; Xiao Hui et al., 2013; Ren Zhanli et al., 2015; Huang Zhigang et al., 2016; Qi Kai et al., 2017), less attention has been devoted to dating the poorly constrained contractional structures. For this study, we focus on the Laolongshan-Shengrenqiao Fault (LSF) cropping out in the southernmost portion of the Ordos Basin. The LSF has been interpreted as a result of Yanshanian intracontinental deformation (Chen Gang and Zhou Dingwu, 1994) or a boundary of the Indosinian-Yanshanian Qinling Orogenic Collage and North China plate (Zhou Dingwu et al., 2002). Here we use AFT thermochronology to constrain the timing of deformation of the LSF. The results will help us determine the timing and displacement of the LSF and understand the interaction between the Qinling Orogenic Collage and Ordos Basin.

2 Geological Background

2.1 Tectonic setting

The Ordos Basin, located in the western block of the North China Plate/Craton (NCC), is the second largest sedimentary basin in China, encompassing an area of about 250, 000 km^2. It is surrounded by the Qinling Orogenic Collage in the south, the Yinshan-Yanshan tectonic belt in the north, the Lvliang Mountain in the east, the Qilian Orogenic Collage in the southwest (Fig. 1). The Ordos Basin is a large intraplate basin with multi-stage evolutionary history (Ritts et al., 2009).

After the finial cratonization of the NCC at approximately 1.82 Ga (Zhai Mingguo, 2011; Liu Chaohui et al., 2012), the Ordos area began to develop sedimentary cover (Lu et al., 2008) and experienced multiple tectono-sedimentary evolutionary phases. The Meso-Neoproterozoic volcaniclastic and carbonate sediments are the first sedimentary cover in the Ordos area during intracontinental rifting and aulacogen development period (Zhai et al., 2014; Chen Youzhi et al., 2016; Gong Wangbin et al., 2016). Subsequently, the Ordos area experienced a long-term denudation (He et al., 2017) and then stepped into a cratonic evolutionary stage during the latest Neoproterozoic to Early Paleozoic (Yang et al., 2005; Bai Yunlai et al., 2013). During the Middle Ordovician to Early Carboniferous, the Ordos area

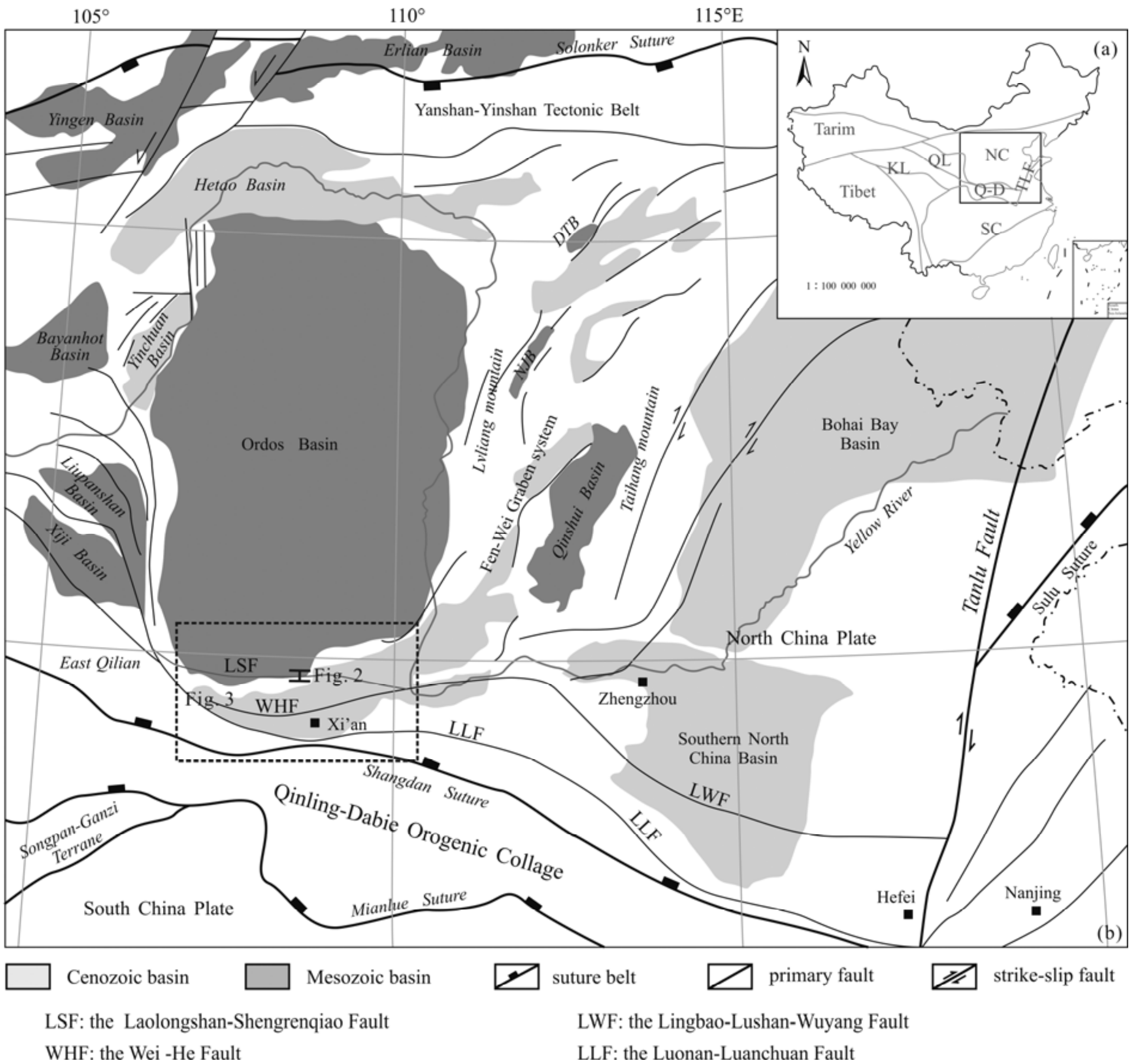

Fig. 1. Regional tectonics and Mesozoic-Cenozoic basins distribution of the North China Plate and its adjacent regions (modified from Darby and Ritts, 2002) (China basemap after China National Bureau of Surveying and Mapping Geographical Information). KL, Kunlun Orogenic Collage; NC, North China; Q-D, Qinling-Dabie Orogenic Collage; QL, Qilian Orogenic Collage; SC, South China; TLF, Tancheng-Lujiang Fault; NJB, Ningwu-Jingle Basin; DTB, Datong Basin.

experienced a long-term of uplift and denudation again (Yang et al., 2005). Then, it subsided and evolved as an intracratonic basin during the Late Paleozoic to Middle Triassic (Yang et al., 2015; Yang Minghui et al., 2015). During latest Middle Triassic to Late Triassic, tectonic differentiation of the NCC occurred initially, as evidenced by the denudation of the eastern NCC and the rapid subsidence of the Ordos Basin (Liu Chiyang et al., 2008; Zhao Junfeng et al., 2009; Yang Minghui et al., 2015). After the latest Triassic to Early Jurassic uplift, tectonic differentiation of the NCC further strengthened and the Middle Jurassic to Early Cretaceous subsidence of Ordos Basin was interrupted by a transient tectonic uplift event at the Late Jurassic (Liu Chiyang et al., 2008; Zhang Yueqiao et al., 2011; Yang Minghui et al., 2015). Later, the convergence of the Pacific Ocean Plate and the Indian-Australian Plate toward the Eurasia Plate further complicated the Ordos Basin, and as such most of this region lacks Late Cretaceous to early Miocene sediments, except for the western part (Li and Li, 2008). Contrary to the hinterland of Ordos Basin, its periphery experienced intense rifting during Cenozoic, resulting in the formation of the grabens.

2.2 The southern Ordos Basin and the LSF

The southern Ordos Basin is separated from Qinling Orogenic Collage by Cenozoic Weihe Graben to the south. This area has been deeply influenced by the pre-Cenozoic multi-cycle orogenesis of Qinling Orogenic Collage (Meng and Zhang, 1999, 2000; Dong et al., 2016), as indicated by polyphase contractional structures (Chen Gang and Zhou Dingwu, 1994). The E-W-trending LSF, cropping out in the southernmost portion of the Ordos Basin, is a polyphase fault (Fig. 2a), which experienced pre-Cenozoic tectonic contraction and Cenozoic negative inversion (Yang Chenyi, 2015). The hanging-wall of the LSF consists of a series of N-vergent folds and thrusts in Paleozoic rocks, while the foot-wall consists of undeformed Triassic rocks (Fig. 2). In addition, the hanging-wall of the LSF is separated from the Cenozoic Weihe Graben by the Kouzhen-Guanshan Fault (Figs. 2a-b). Due to the lack of the constraints from overlying younger undeformed strata, the E-W-trending LSF has previously been interpreted as a part of Yanshanian tectonics (Chen Gang and Zhou Dingwu, 1994), which is usually characterized by ENE-SSW-trending thrusts and folds (Qi Kai et al., 2017).

2.3 Previous AFT thermochronological work

Previous thermochronological studies (Chen Gang et al., 2007; Wang Jianqiang et al., 2010; Xiao Hui et al., 2013; Ren Zhanli et al., 2015; Huang Zhigang et al., 2016; Qi Kai et al., 2017) have reported a few AFT data aiming to constrain the exhumation processes of the southern Ordos Basin. Reviewing and compiling the reported AFT data, we found that some of them failed the χ^2 test, suggesting that the reported apparent ages could not constrain the timing of exhumation although they are significantly younger than the corresponding depositional ages. In Fig. 3, we summarized published AFT data with P (χ^2) >5% and the apparent age younger than the corresponding depositional age. The previously published AFT data were mainly distributed in the foot-wall of the LSF, and only one sample (Kz-2a) was collected from the hanging-wall. The wide range of the reported AFT ages (38–125 Ma) suggest various magnitudes of exhumation affecting different parts of the southern Ordos Basin. In addition, it is worth noting that the AFT ages from opposite sides of the LSF at Kouzhen section, 63 Ma for the foot-wall sample (Kz-1) and 59 Ma for the hanging-wall sample (Kz-2a), are almost equal. However, our two unpublished apatite (U-Th-Sm)/He ages from the hanging-wall samples of the LSF at Kouzhen section are 57.4 Ma and 63.7 Ma, implying that the previously published AFT data for the hanging-wall sample (Kz-2a) of the LSF is suspicious. We seek to get accurate AFT ages from

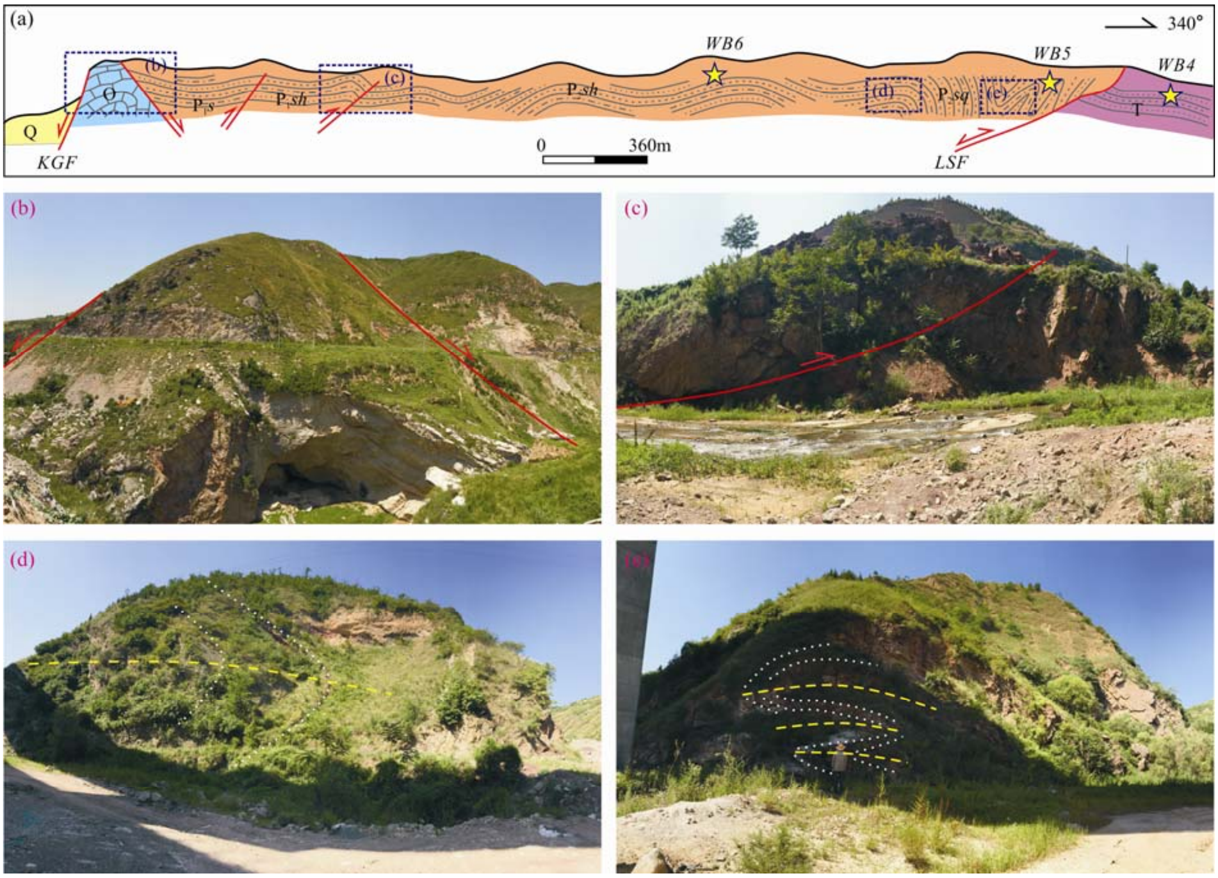

Fig. 2. (a), Schematic cross section showing deformation characteristics of the LSF at Kouzhen section (modified from Chen Gang and Zhou Dingwu, 1994); (b), The Kouzhen-Guanshan Fault (KGF), the northern boundary fault of Cenozoic Weihe Graben, and the normal fault in the hanging-wall of the LSF; (c), N-vergent thrust in the hanging-wall of the LSF; (d) and (e) Recumbent folds in the hanging-wall of the LSF.

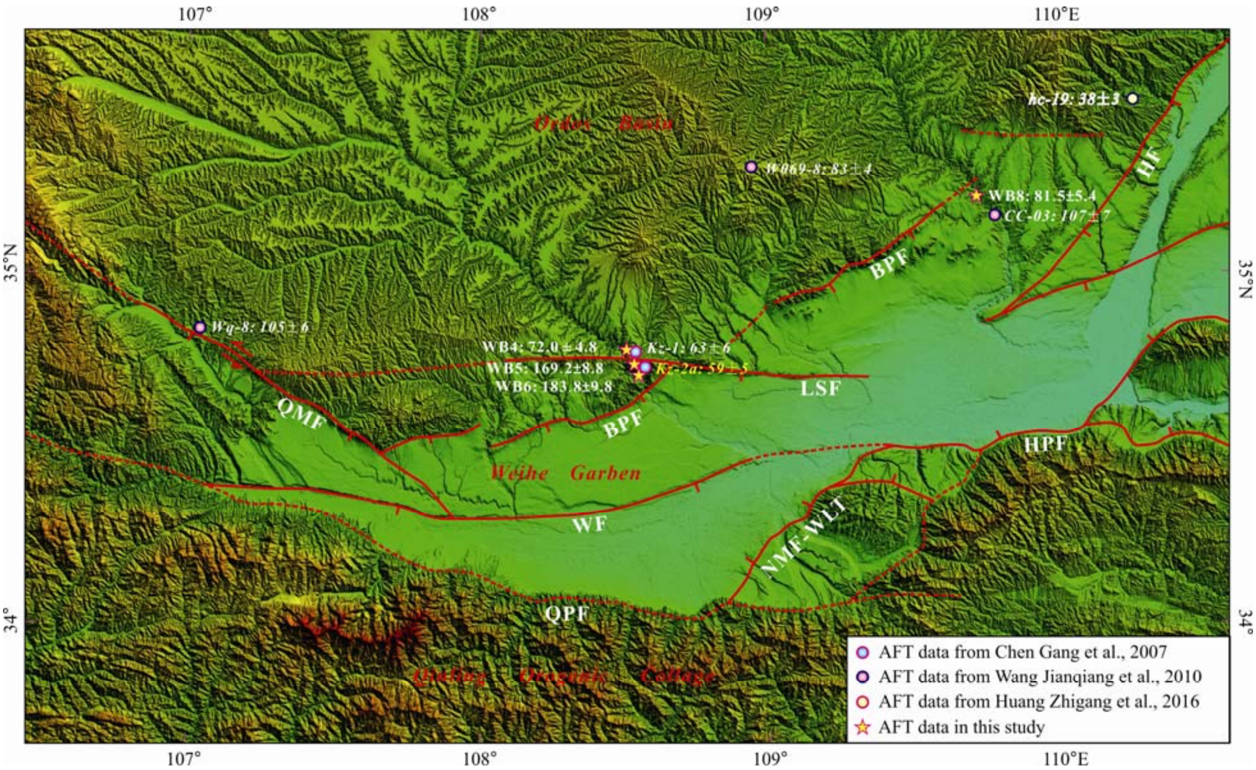

Fig. 3. Digital elevation model (DEM) and previous published AFT data of the southern Ordos Basin.
AFT age data are sourced from Chen Gang et al. (2007), Wang Jiangqiang et al. (2010), Huang Zhigang et al. (2016) and this study. HF, Hancheng Fault; HPF, Huashan Piedmont Fault; NMF-WLT, North Margin Fault of the Weinan Loess Tableland; BPF, Beishan Piedmont Fault; QPF, Qinling Piedmont Fault; KGF, Kouzhen-Guanshan Fault; WF, Weihe Fault; QMF, Qishan-Mazhou Fault.

opposite sides of the LSF and to provide thermochronological constraints on the timing and displacement of the LSF.

3 Samples and Methods

In general, the timing of tectonic contraction and associated hanging-wall exhumation is synchronous with the onset of rapid cooling. Therefore, reasonable sampling for low-temperature thermochronology study could provide the tightest constraint on timing of tectonic contraction and thrust fault activity. In this study, 9 sandstone samples (Table 1; Fig. 3), 3 kg each, were collected from both hanging-wall and foot-wall of the LSF in the southern Ordos Basin. Enough apatite grains for AFT analysis were successfully separated from 4 of 9 samples, using standard heavy liquid and magnetic separation techniques. Three of them were collected at the Kouzhen section, including two hanging-wall samples and one foot-wall sample; while another foot-wall sample is located 100 km apart from Kouzhen section, albeit seemed slightly distant, deformation structure between them can be ruled out due to the lack of transverse structure in the southern Ordos Basin (Zhou Dingwu et al., 2002; Qi Kai et al., 2017). According to apatite yields and quality, apatite fission track analysis was conducted on four samples by LA-ICP-MS method at University of Melbourne, following analytical details based on Gleadow et al. (2015). Experimental procedures for this method are described briefly below.

Apatite grains were mounted in epoxy resin on glass slides. Mounts were then ground to expose internal grain surfaces and polished to an optical finish, prior to etching in 5N HNO_3 for 20 seconds at 20°C to reveal the fossil tracks. The polished and etched mounts were also coated with a thin Au film (~10 nm) to enhance the surface reflectivity and minimizes internal reflections under the microscope (Gleadow et al., 2009). Apatite grains with c-

Table 1 Sample information for low temperature thermochronology in the southern Ordos Basin.

Sample ID	Lithology	Strata	Longitude (E)	Latitude (N)	Elevation (m)
WB4	Sandstone	Lower Triassic	108°40′59″	34°44′38″	674
WB5	Sandstone	Upper Permian	108°41′29″	34°44′11″	652
WB6	Sandstone	Lower Permian	108°41′31″	34°44′07″	649
WB8	Sandstone	Upper Permian	109°43′07″	35°13′34″	524

axes lying horizontally in the plane of the polished surface, relatively homogeneous track distributions, with minimal dislocations and other surface imperfections, were selected for counting using circular polarised light and an automated grain detection option in TrackWorks. Reflected and transmitted light digital image sets were then captured autonomously and analyzed offline using FastTracks image processing software. Spontaneous fission tracks were counted automatically using the coincidence mapping procedure described by Gleadow et al. (2009) and then manually corrected as necessary. The c -axis direction was determined automatically and corrected manually as necessary. Average Dpar values (Donelick et al., 2005) for all single track etch pits were also determined automatically. Confined track length measurements were made on c-axis parallel grains as true 3D lengths using captured digital images. Confined lengths were measured per sample as more as possible. ^{252}Cf tracks were implanted into polished grains to enhance the number of confined track intersections below the surface (Donelick and Miller, 1991). After counting, uranium concentrations were measured by LA-ICP-MS using a New Wave UP-213 Quintupled Nd: YAG Laser Microprobe and an Agilent 7700X ICP-MS. For each apatite grain a laser spot of 30 μm diameter was ablated to a depth of ~8 μm in a 'Supercell' under He, with Ar as the carrier gas. The 213 nm laser was used with a pulse rate of 5 Hz and 45% power giving an energy density of 2.3 J/cm^2 at the target. Measurements were made on the $^{238}U/^{43}Ca$ ratio against glass (NIST612) and a homogenized and recrystallized Mud Tank Carbonatite apatite standard. Repeat analyses of a Durango apatite reference crystal were also included with the FCT runs as an additional internal standard. Lastly, fission track ages were calculated from the spontaneous track densities and single grain ^{238}U concentrations as described by Hasebe et al. (2004).

To help interpret the AFT data, thermal history modeling was performed using the inverse Monte-Carlo modelling approach of HeFTy 1.9.1 (Ketcham, 2005), which uses the Kolmogorov-Smirnov test to assess the fit between modeled and measured data (Ketcham, 2005), thus ruling out the inappropriate models (Vermeesch and Tian, 2014). In this study, AFT data are modeled using the multi-kinetic annealing model of Ketcham et al. (2007), with Dpar values as a kinetic parameter. Depending on the AFT data (i.e. ages and lengths) and the geological evolution of the southern Ordos Basin, constraints used for inversion modeling were as follow: (a) The starting time was constrained by the deposition ages of the rock samples and assuming that the paleo-surface temperature was 20±10°C; (b) A broad temperature constraint of 120–180°C was set at a time older than the corresponding apparent AFT age; and (c) A present-day mean surface temperature of 20±10°C provided the final constraint. These pre-modeling settings always contain large uncertainties in order to give the inversion algorithm sufficient freedom to search for a wide range of possible thermal histories. In this study, inverse modeling was run randomly until 500 good paths were obtained, which resulted in >4000 acceptable paths, such that sufficient model paths were available to clearly differentiate between "good fit" and "acceptable fit" solutions.

4 Results

4.1 AFT data

The AFT data set including age, length, and Dpar are presented in Table 2. Radial plots of single grain age data are illustrated in Fig. 4. The AFT ages range from 72.0±4.8 to 183.8±9.8 Ma, and all are significantly younger than their stratigraphic ages and therefore considered to have been fully thermally reset. All samples passed the χ^2 test (Galbraith, 1981), showing the homogeneity of the grain age population. Spreading of individual grain ages may result from different chemical compositions of the apatite grains, although there is no clear correlation between Dpar values and AFT ages (Fig. 5). The mean Dpar values vary between 1.45 μm and 1.72 μm, indicating fairly similar chemical compositions with a low resistance to annealing (Ketcham et al., 1999). The mean length of confined tracks ranges between 11.9±0.2 μm and 12.5±0.4 μm, with standard deviations of 0.13 to 2.29 μm, suggesting a slow exhumation or a prolonged residence in the APAZ.

The AFT ages for the hanging-wall and foot-wall samples from across the LSF are distinctly different and are out of analytical error, indicating that they have experienced contrasting exhumation history. Hanging-wall samples, WB5 and WB6, yielded AFT ages of 169.2±8.8

Table 2 LA-ICP-MS-based AFT data for sandstone samples from the southern Ordos Basin

Sample ID	No. of grains	Ns	$\rho s(10^5\ cm^{-2})$	Pooled ^{238}U (ppm±1σ)	D_{par} (μm)	Pooled age (Ma±1σ)	$P(\chi^2)$ (%)	Dispersion (%)	Central age (Ma±1σ)	N_{length}	Mean trackLength (μm ± se)	SD (μm)
WB4	6	311	7.3054	23.09±12.77	1.45	72.0±4.8	21.06	0	72.6±4.6	2	12.5±0.1	0.13
WB5	16	1920	13.0309	17.16±11.22	1.50	169.2±8.8	15.93	12	172.9±7.6	71	11.9±0.2	1.66
WB6	12	941	20.2514	23.42±15.87	1.68	183.8±9.8	24.05	5	185.6±7.9	25	12.3±0.4	1.89
WB8	21	2174	17.8349	46.58±36.43	1.72	81.5±5.4	45.43	26	81.3±5.3	27	12.5±0.4	2.29

Note:Ns = number of spontaneous tracks counted; ρs = spontaneous track density; D_{par} = long axis of track etch pit; N_{length}= number of lengths measured; se = standard error.

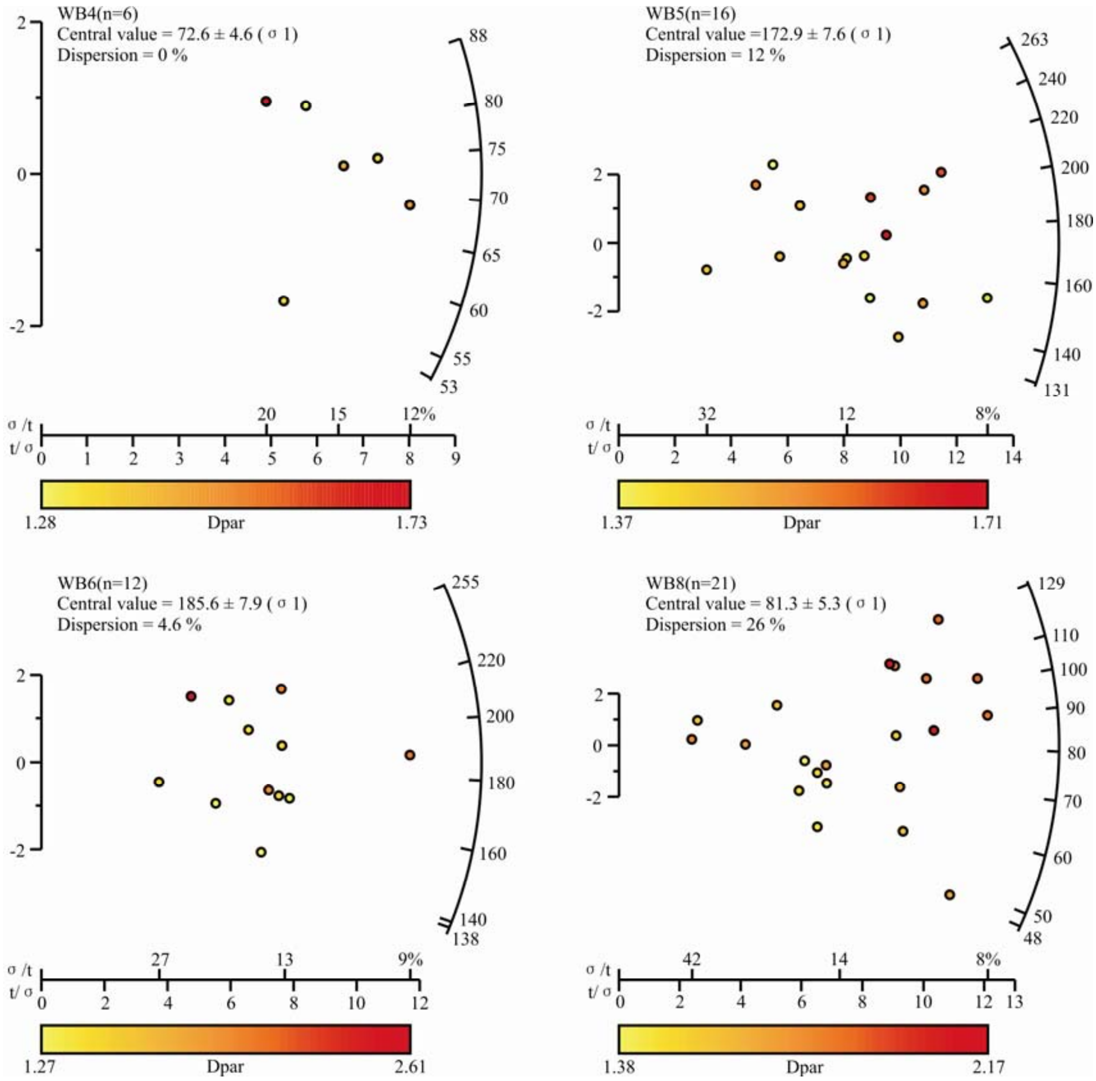

Fig. 4. Radial plots of calculated AFT cooling ages for samples in this study.

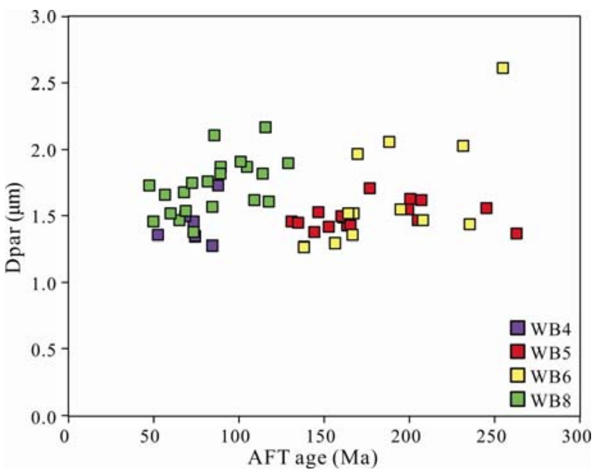

Fig. 5. Dpar vs. single-grain AFT age plot is given for samples in this study.

Ma and 183.8±9.8 Ma, respectively, while the foot-wall samples, WB4 and WB8, yielded younger AFT ages of 72.0±4.8 Ma and 81.5±5.4 Ma, respectively (Fig. 4; Table 2). Despite the results analyzed by different methods, our results for the foot-wall samples agree well with the previously published results (Fig. 3), suggesting that both of the analytical methods are reliable and the results could be discussed together. However, it is worth noting that the new AFT ages for the hanging-wall of the LSF are significantly older than the previously published AFT age (Kz-2a), and furtherly provides new evidence for the incorrectness of the reported AFT age.

4.2 Thermal history modeling

In order to further constrain the evolution of the LSF, thermal history modeling has been conducted to reconstruct the time-temperature histories (t–T evolution) of hanging-wall and foot-wall samples, respectively. Fig. 6 shows the results of HeFTy Monte-Carlo simulations that were run for hanging-wall and foot-wall samples from the LSF, in the southern Ordos Basin.

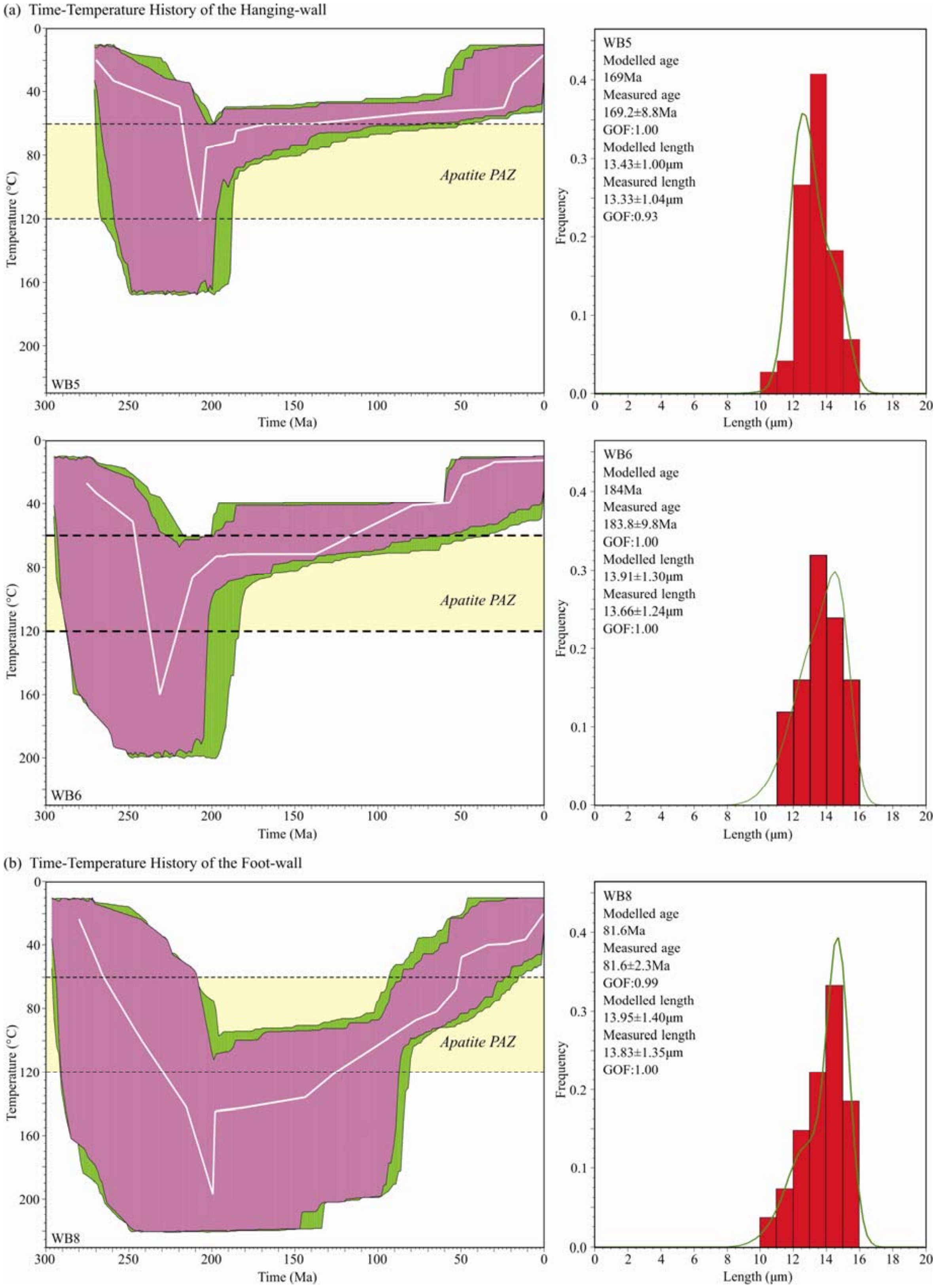

Fig. 6. Low-temperature thermal history models for representative hanging-wall and foot-wall samples of the LSF. Models were constructed using the modelling software HeFTy (Ketcham, 2005).

Note that modelled t-T paths are valid only inside 120–60°C (APAZ). Outside this temperature range, the actual sample thermal trajectory is not presented unless constrained by other data.

As can be seen from Fig. 6, the hanging-wall and foot-wall samples both have been reheated after deposition to temperatures higher than the AFT closure temperature. Then, the hanging-wall samples (WB5 and WB6) entered into the APAZ and were fastly brought to the upper part of APAZ at ~205–185 Ma. While the foot-wall sample (WB8) experienced a long period at the lower part of APAZ and was fastly brought out the APAZ at ~85–60 Ma. In addition, the time-temperature histories of WB5, WB6 and WB8 all apparently detect a Cenozoic accelerated cooling event, because the cooling pathways are mostly located outside the APAZ (i.e. <60°C), where thermal modelling is invalid and should not be overly interpreted.

5 Discussions

5.1 Timing and displacement of thrusting of the LSF

The data obtained in this study reveal a significant AFT age discontinuity across the LSF, which provide us a good opportunity to determine deformation timing of the LSF. Because all single grain ages are significant younger than their stratigraphic ages, the AFT ages obtained in this study all stand for cooling age. The hanging-wall AFT ages of the LSF indicate these rocks have cooled below apatite closure temperature (110°±10°C) between ~190–170 Ma. In contrast, the foot-wall AFT ages imply these rocks have cooled below apatite closure temperature (110°±10°C) between ~90–70 Ma. This age discontinuity suggests a significant thermal contrast existed in the rocks now juxtaposed along the LSF at least since Early Jurassic. Moreover, the thermal history modeling indicates that this thermal contrast existed along the LSF initially formed at the latest Triassic.

Regarding the displacement of thrusting of the LSF, the thermal modeling indicates a ~50°C difference in temperature between opposite sides of the LSF at the latest Triassic to Early Jurassic. This difference in temperature corresponds to ~1.7 km of net vertical displacement along the LSF if a linear steady-state geothermal gradient of 30°C/km is assumed. Therefore, the observed AFT age discontinuity is best explained by an episode of thrusting and exhumation of the LSF with ~1.7 km of net vertical displacement during the latest Triassic to Early Jurassic.

5.2 Regional implications

Previous studies suggest that there was a depositional hiatus and differential denudation event within the Ordos Basin during the latest Triassic to Early Jurassic (Liu Chiyang et al., 2008; Chen Gang et al., 2007; Yang et al., 2015; Yang Minghui et al., 2015). Regarding the tectonic regime of this event, however, essential questions still remain unsolved. Although it may be a response to the Early Mesozoic collision and the continued compression of the South Qinling and the South China Plate along the Mianlue Suture, which finally combinated the NCC, the South Qinling, and the South China Plate, critical evidence is missing because most original tectono-sedimentary records related this tectonic event have been deeply buried beneath the Weihe Graben by Cenozoic intense subsidence. In this work, the determination of the latest Triassic to Early Jurassic thrusting and exhumation of the LSF in the southern Ordos Basin provides an opportunity to reassess coeval tectonic regime.

The stratigraphic contact relationship of the southern Ordos Basin suggests that this region experienced a differential denudation processes during the latest Triassic to Early Jurassic, characterized by parallel unconformity between the Triassic and Jurassic strata in the hinterland of Ordos Basin, whereas high-angle unconformity in the periphery (Fig. 7), implying that the periphery experienced a stronger coeval tectonic deformation and denudation processes. In this study, the determination of coeval thrusting of the LSF suggests that the latest Triassic to Early Jurassic differential denudation can be confidently ascribed to tectonic stress propagation derived from the continued compression of Qinling Orogenic Collage. Moreover, the determination of the latest Triassic to Early Jurassic thrusting of the LSF also implies that there may be a coeval north-vergent fold-and-thrust belt between the Ordos Basin and the Qinling Orogenic Collage although the main body of it has been deeply buried beneath the Cenozoic Weihe Graben, and the LSF might act as the thrust front of this north-vergent fold-and-thrust belt.

Additionally, the Mesozoic exhumation history of the southern Ordos Basin is still in dispute. Wang Jianqiang et al. (2010) suggested the exhumation of the southern Ordos Basin mainly occurred in the Late Cretaceous, while Qi Kai et al. (2017) demonstrated that there was a Late Jurassic to earliest Cretaceous thrust-driven exhumation prior to Late Cretaceous overall exhumation. The main reason for this dispute is that the samples of these studies are mostly limited to certain geographic regions. Synthesizing thermochronological data (Fig. 3), stratigraphic contact relationship (Fig. 7), and tectono-sedimentary evolution (Fig. 8), here we suggest that the southern Ordos Basin experienced a multi-stage differential exhumation during Mesozoic, including the latest Triassic to Early Jurassic and Late Jurassic to earliest Cretaceous thrust-driven exhumation as well as Late Cretaceous overall exhumation.

As discussed in Section 5.1, new AFT data in this study, together with stratigraphic contact relationship between the Triassic and Jurassic strata (Fig. 7), provide

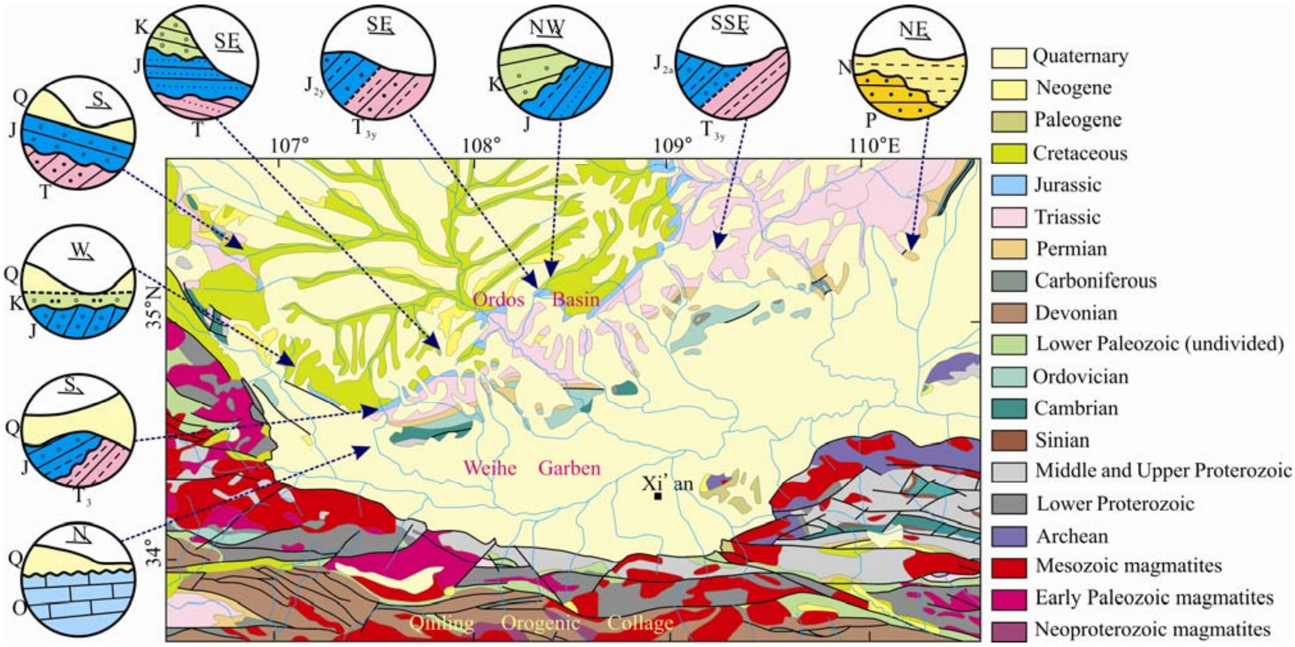

Fig. 7. Geological map and stratigraphic contact relationship of the southern Ordos Basin.
Partial data are modified from Gao Fei (2009) and Tang Xiyuan et al. (1992).

unambiguous evidence for the latest Triassic to Early Jurassic thrust-driven exhumation in the southern Ordos Basin, which act as a response to the Early Mesozoic collision and the continued compression of the South Qinling and the South China plate along the Mianlue Suture (Meng and Zhang, 1999, 2000). Then, the Ordos Basin entered into an oblique extensional tectonic setting, as the result of the NW-trending subduction of the Izanagi Plate toward the NCC (Faure et al., 2012; Yang et al., 2015). During the Late Jurassic to earliest Cretaceous, the southern Ordos Basin experienced a more intense thrust-driven exhumation event, evidenced by well-preserved fold-and-thrust belt style deformation, widespread angular unconformity between the Jurassic and Cretaceous strata, coeval coarse-grained sedimentation and depositional hiatus (Qi Kai et al., 2017). From the viewpoint of regional tectonics, this thrust-driven exhumation event was controlled by the coeval intracontinental southward subduction of the NCC and continuously northward subduction of the South China Plate beneath the Qinling Orogenic Collage (Dong et al., 2016). From the viewpoint of plate tectonics, this tectonic event recorded the far-field effects of multiple plate interactions, including the paleo-Pacific Plate subduction along the eastern margin of the East Asia, the collision between the Qiangtang and Lhasa Plates, and the convergence between the Mongol-China and the Siberia Plates (Dewey et al., 1988; Yin and Nie, 1996; Dong et al., 2015). After the Early Cretaceous weak subsidence, shrinking and vanishing of the Ordos basin occurred at the Late Cretaceous, characterized by long-term basin-scale exhumation, which was related to the collision of an exotic terrain with the eastern margin of continental China at ~100 Ma (Niu et al., 2015; Ding et al., 2017).

6 Conclusions

The LA-ICP-MS-based AFT method can be used to date rock exhumation that accompany fault activity. In this study, we performed an AFT thermochronology to unravel the timing of thrusting and exhumation for the LSF in the southern Ordos Basin, and the following conclusions can be drawn:

(1) The AFT ages from opposite sides of the LSF reveal a significant latest Triassic to Early Jurassic time-temperature discontinuity across the structure. Hanging-wall samples yielded AFT ages of 169.2±8.8 Ma and 183.8±9.8 Ma, while the foot-wall samples yielded AFT ages of 72.0±4.8 Ma and 81.5±5.4 Ma. Modeling of track length distributions reveals at the latest Triassic to Early Jurassic, a ~50°C difference in temperature between opposite sides of the LSF currently exposed at the surface. This discontinuity is best interpreted by an episode of thrusting and exhumation of the LSF with ~1.7 km of net vertical displacement during the latest Triassic to Early Jurassic.

(2) The latest Triassic to Early Jurassic thrusting and exhumation the LSF suggests that the southern Ordos Basin experienced coeval intense tectonic deformation and developed a north-vergent fold-and-thrust belt. And the

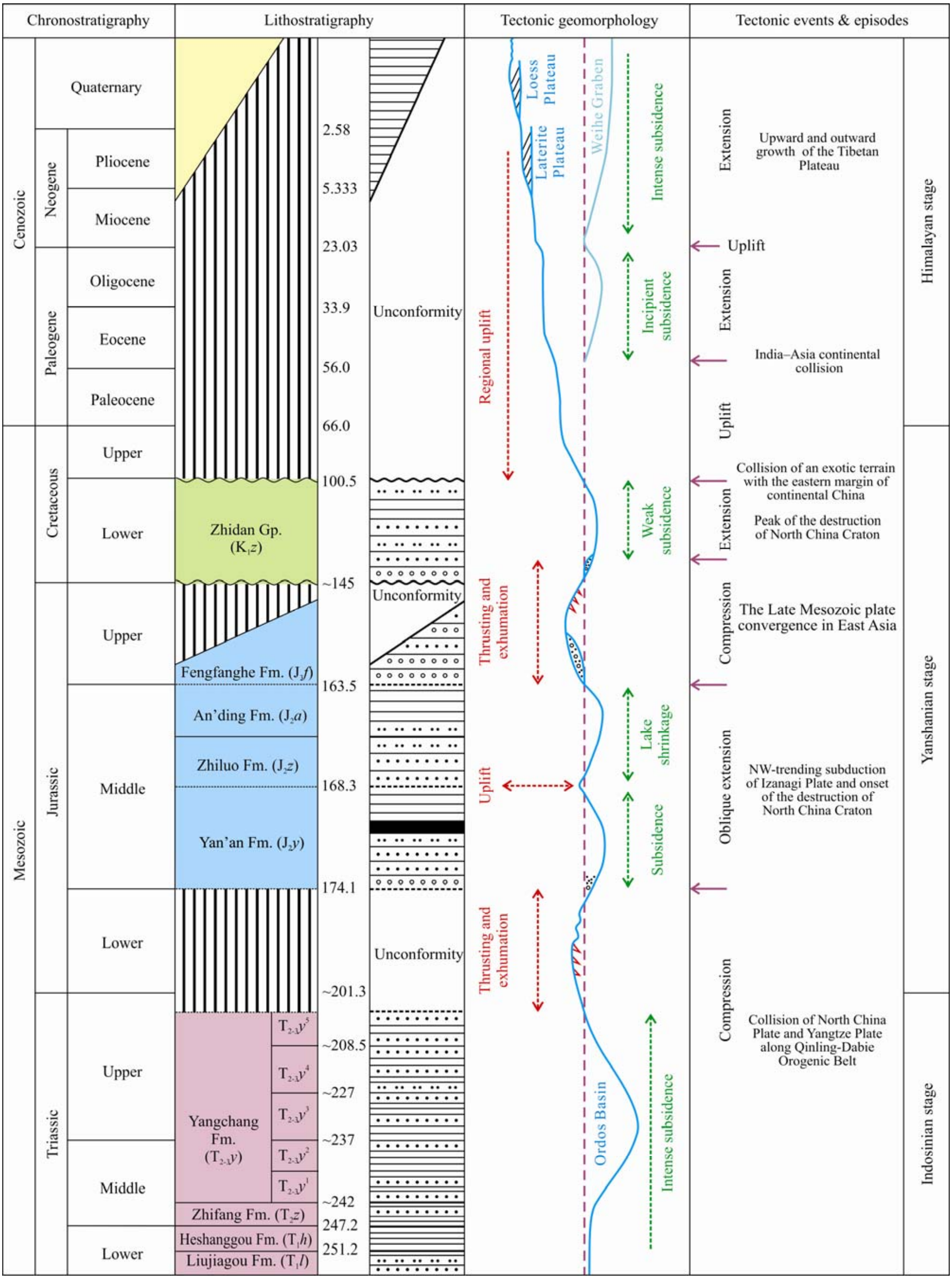

Fig. 8. Summary of the Meso–Cenozoic tectonic evolution of the southern Ordos Basin (modified from Liu Chiyang et al., 2008; Yang et al., 2015).

LSF was the thrust front of this north-vergent fold-and-thrust belt. When combined with earlier structural and thermochronological studies, these results suggest the southern Ordos Basin experienced a multi-stage differential exhumation during Mesozoic, including the latest Triassic to Early Jurassic and Late Jurassic to earliest Cretaceous thrust-driven exhumation as well as Late Cretaceous overall exhumation. Specifically, the two thrust-driven exhumation events were related to tectonic stress propagation derived from the latest Triassic to Early Jurassic continued compression in Qinling Orogenic Collage and Late Jurassic to Early Cretaceous intracontinental orogeny of Qinling Orogenic Collage, respectively. By contrast, Late Cretaceous overall exhumation event was related to the collision of an exotic terrain with the eastern margin of continental China at ~100 Ma.

Acknowledgements

We thank Prof. Barry P. Kohn of University of Melbourne for his help with the sample tests. Li Yiwei and Jia Chunyang participated in some of the field works. We thank the anonymous reviewer and the Editor for their comments and suggestions, which significantly improved the quality of the manuscript. This work was supported by the National Natural Science Foundation of China (Grants No. 41572102, 41330315, 41102067, and 41172127) and China Geological Survey project (Grant No. 121201011000161111-02).

Manuscript received Feb. 25, 2018
accepted May. 10, 2018
edited by Liu Lian

References

Bai Yunlai, Ma Yuhu, Huang Yong, Liao Jianbo and Liu Xiaoguang, 2013. Properties of continental margin and its hydrocarbon exploration significance in Cambrian in the Southern Ordos Kratogen of North China. *Acta Geologica Sinica* (English Edition), 88(3): 777–803.

Bande, A., Sobel, E.R., Mikolaichuk, A., Schmidt, A., and Stockli, D.F., 2017. Exhumation history of the western Kyrgyz Tien Shan: Implications for intramontane basin formation. *Tectonics*, 36(1): 163–180.

Blythe, A.E., and Longinotti, N., 2013. Exhumation of the southern Sierra Nevada–eastern Tehachapi Mountains constrained by low-temperature thermochronology: Implications for the initiation of the Garlock fault. *Lithosphere*, 5(3): 321–327.

Chen Gang and Zhou Dingwu, 1994. Geological significance and characteristics of the covering strata deformation in Kouzhen-Shengrenqiao, Chunhua county, Shaanxi province. *Journal of Northwest University* (Natural Science Edition), 24(2): 163–166 (in Chinese with English abstract).

Chen Gang, Sun Jianbo, Zhou Lifa, Zhang Huiruo, Li Xiangping and Wang Zhiwei, 2007. Fission-track-age records of the Mesozoic tectonic-events in the southwest margin of the Ordos Basin, China. *Science in China* (Series D: Earth Sciences), 50(suppl. 2): 133–143.

Chen Youzhi, Fu Jinhua, Yang Gaoyin, Xiao Ancheng, Sun Liuyi, Xu Bo, Bao Hongping and Mao Liguang, 2016. Researches on basin property of Ordos block during Mesoproterozoic Changcheng Period. *Acta Petrologica Sinica*, 32(3): 856–864 (in Chinese with English abstract).

Cheng Xiaogan, Lin Xiubin, Wu Lei, Chen Hanlin, Xiao Ancheng, Gong Junfeng, Zhang Fengqi and Yang Shufeng, 2016. The Exhumation History of North Qaidam Thrust Belt Constrained by Apatite Fission Track Thermochronology: Implication for the Evolution of the Tibetan Plateau. *Acta Geologica Sinica* (English Edition), 90(3): 870–883.

Darby, B.J., and Ritts, B.D., 2002. Mesozoic contractional deformation in the middle of the Asian tectonic collage: The intraplate Western Ordos fold-thrust belt, China. *Earth and Planetary Science Letters*, 205(1–2): 13–24.

Dewey, J.F., Shackleton, R.M., Chang, C., and Sun, Y., 1988. The Tectonic Evolution of the Tibetan Plateau. *Philosophical Transactions of the Royal Society A: Mathematical, Physical and Engineering Sciences*, 327(1594): 379–413.

Dielforder, A., Berger, A., and Herwegh, M., 2016. The accretion of foreland basin sediments during early stages of continental collision in the European Alps and similarities to accretionary wedge tectonics. *Tectonics*, 35(10): 2216–2238.

Ding, W., Li, J., Wu, Z., Li, S., and Lin, X., 2017. Late Mesozoic transition from Andean-type to Western Pacific-type of the East China continental margin—Is the East China Sea basement an allochthonous terrain? *Geological Journal*. (In press)

Donelick, R.A., 2005. Apatite Fission-Track Analysis. *Reviews in Mineralogy and Geochemistry*, 58(1): 49–94.

Donelick, R.A., and Miller, D.S., 1991. Enhanced tint fission track densities in low spontaneous track density apatites using 252Cf-derived fission fragment tracks: A model and experimental observations. *International Journal of Radiation Applications and Instrumentation*, Part 18(3): 301–307.

Dong, S., Zhang, Y., Zhang, F., Cui, J., Chen, X., Zhang, S., Miao, L., Li, J., Shi, W., Li, Z., Huang, S., and Li, H., 2015. Late Jurassic-Early Cretaceous continental convergence and intracontinental orogenesis in East Asia: A synthesis of the Yanshan Revolution. *Journal of Asian Earth Sciences*, 114: 750–770.

Dong, Y., Yang, Z., Liu, X., Sun, S., Li, W., Cheng, B., Zhang, F., Zhang, X., He, D., and Zhang, G., 2016. Mesozoic intracontinental orogeny in the Qinling Mountains, central China. *Gondwana Research*, 30: 144–158.

Du Jianjun, Li Dunpeng, Wang Yufang and Ma Yinsheng, 2017. Late Quaternary Activity of the Huashan Piedmont Fault and Associated Hazards in the Southeastern Weihe Graben, Central China. *Acta Geologica Sinica* (English Edition), 91 (1): 76–92.

Duvall, A.R., Clark, M.K., van der Pluijm, B.A., and Li, C., 2011. Direct dating of Eocene reverse faulting in northeastern Tibet using Ar-dating of fault clays and low-temperature thermochronometry. *Earth and Planetary Science Letters*, 304 (3–4): 520–526.

Ehlers, T.A., Armstrong, P.A., and Chapman, D.S., 2001. Normal fault thermal regimes and the interpretation of low-temperature thermochronometers. *Physics of the Earth and Planetary Interiors*, 126(3–4): 179–194.

Faure, M., Lin, W., and Chen, Y., 2012. Is the Jurassic (Yanshanian) intraplate tectonics of North China due to westward indentation of the North China block? *Terra Nova*, 24(6): 456–466.

Fitzgerald, P.G., Duebendorfer, E.M., Faulds, J.E., and O'Sullivan, P., 2009. South Virgin-White Hills detachment fault system of SE Nevada and NW Arizona: Applying apatite fission track thermochronology to constrain the tectonic evolution of a major continental detachment fault. *Tectonics*, 28(2): TC2001.

Galbraith, R.F., 1981. On statistical models for fission track counts. *Journal of the International Association for Mathematical Geology*, 13(6): 471–478.

Gao Fei, 2009. *Meso-Cenozoic structural characteristics and its evolution and reformation in Weibei area*. Xi'an: Northwest University (Master's Thesis): 1–80 (in Chinese with English abstract).

Gautheron, C., Espurt, N., Barbarand, J., Roddaz, M., Baby, P., Brusset, S., Tassan-Got, L., and Douville, E., 2013. Direct dating of thick- and thin-skin thrusts in the Peruvian Subandean zone through apatite (U-Th)/He and fission track thermochronometry. *Basin Research*, 25(4): 419–435.

Giorgis, S., Weber, J., Sanguinito, S., Beno, C., and Metcalf, J., 2017. Thermochronology constraints on Miocene exhumation in the Central Range Mountains, Trinidad. *Geological Society of America Bulletin*, 129(1–2): 171–178.

Gleadow, A., Harrison, M., Kohn, B., Lugo-Zazueta, R., and Phillips, D., 2015. The Fish Canyon Tuff: A new look at an old low-temperature thermochronology standard. *Earth and Planetary Science Letters*, 424: 95–108.

Gleadow, A.J.W., Duddy, I.R., and Lovering, J.F., 1983. Fission track analysis: a new tool for the evaluation of thermal histories and hydrocarbon potential. *The APPEA Journal*, 23 (1): 93–102.

Gleadow, A.J.W., Gleadow, S.J., Belton, D.X., Kohn, B.P., Krochmal, M.S., and Brown, R.W., 2009. Coincidence mapping - a key strategy for the automatic counting of fission tracks in natural minerals. *Geological Society, London, Special Publications*, 324: 25–36.

Gong Wangbin, Xi Shengli, Liu Xinshe, Hu Jianmin and Li Zhenhong, 2016. LA-ICP-MS U-Pb Dating of Detrital Zircons from Changcheng System in Ordos Block,Western North China Craton and Its Implications. *Geological Review*, 62(6): 1379–1391 (in Chinese with English abstract).

Green, P.F., Duddy, I.R., Laslett, G.M., Hegarty, K.A., Gleadow, A.J.W., and Lovering, J.F., 1989. Thermal annealing of fission tracks in apatite 4. Quantitative modelling techniques and extension to geological timescales. *Chemical Geology* (Isotope Geoscience section), 79(2): 155–182.

Hasebe, N., Barbarand, J., Jarvis, K., Carter, A., and Hurford, A.J., 2004. Apatite fission-track chronometry using laser ablation ICP-MS. *Chemical Geology*, 207(3–4): 135–145.

He, T., Zhou, Y., Vermeesch, P., Rittner, M., Miao, L., Zhu, M., Carter, A., Pogge von Strandmann, P.A.E., and Shields, G.A., 2017. Measuring the 'Great Unconformity' on the North China Craton using new detrital zircon age data. *Geological Society, London, Special Publications*, 448: 145–159.

Holford, S.P., Green, P.F., Duddy, I.R., Turner, J.P., Hillis, R.R., and Stoker, M.S., 2009. Regional intraplate exhumation episodes related to plate-boundary deformation. *Geological Society of America Bulletin*, 121(11–12): 1611–1628.

Huang Zhigang, Ren Zhanli and Gao Longgang, 2016. Evidence from detrital zircon and apatite fission track for tectonic evolution since cretaceous in southeastern margin of Ordos Basin. Chinese *Journal of Geophysics*-Chinese Edition, 59 (10): 3753–3764.

Ketcham, R.A., 2005. Forward and Inverse Modeling of Low-Temperature Thermochronometry Data. *Reviews in Mineralogy and Geochemistry*, 58(1): 275–314.

Ketcham, R.A., Carter, A., Donelick, R.A., Barbarand, J., and Hurford, A.J., 2007. Improved modeling of fission-track annealing in apatite. *American Mineralogist*, 92(5–6): 799–810.

Ketcham, R.A., Donelick, R.A., and Carlson, W.D., 1999. Variability of apatite fission-track annealing kinetics; III, Extrapolation to geological time scales. *American Mineralogist*, 84(9): 1235–1255.

Li, R., and Li, Y., 2008. Tectonic evolution of the western margin of the Ordos Basin (Central China). *Russian Geology and Geophysics*, 49(1): 23–27.

Li, S.Z., Zhao, G.C., Zhang, G.W., Liu, X.C., Dong, S.W., Wang, Y.J., Liu, X., Suo, Y.H., Dai, L.M., Jin, C., Liu, L.P., Hao, Y., Liu, E.S., Wang, J., and Wang, T., 2010. Not all folds and thrusts in the Yangtze foreland thrust belt are related to the Dabie Orogen: Insights from Mesozoic deformation south of the Yangtze River. *Geological Journal*, 45(5–6): 650–663.

Liu Chaohui, Liu Fulai and Zhao Guochun, 2012. Paleoproterozoic basin evolution in the Trans-North China Orogen, North China Craton. *Acta Petrologica Sinica*, 28(9): 2770–2784 (in Chinese with English abstract).

Liu Chiyang, Zhao Hongge, Zhao Junfeng, Wang Jianqiang, Zhang Dongdong and Yang Minghui, 2008. Temporo-spatial Coordinates of Evolution of the Ordos Basin and Its Mineralization Responses. *Acta Geologica Sinica* (English Edition), 82(6): 1229–1243.

Lu, S., Zhao, G., Wang, H., and Hao, G., 2008. Precambrian metamorphic basement and sedimentary cover of the North China Craton: A review. *Precambrian Research*, 160(1–2): 77–93.

Maino, M., Casini, L., Ceriani, A., Decarlis, A., Di Giulio, A., Seno, S., Setti, M., and Stuart, F.M., 2015. Dating shallow thrusts with zircon (U-Th)/He thermochronometry—The shear heating connection. *Geology*, 43(6): 495–498.

Meng Qingren, 2017. Origin of the Qinling Mountains. *Scientia Sinica Terrae*, 47: 412–420 (in Chinese).

Meng, Q.-R., and Zhang, G.-W., 1999. Timing of collision of the North and South China blocks: Controversy and reconciliation. *Geology*, 27(2): 123–126.

Meng, Q.-R., and Zhang, G.-W., 2000. Geologic framework and tectonic evolution of the Qinling orogen, central China. *Tectonophysics*, 323(3–4): 183–196.

Merten, S., Matenco, L., Foeken, J.P.T., and Andriessen, P.A.M., 2011. Toward understanding the post-collisional evolution of an orogen influenced by convergence at adjacent plate margins: Late Cretaceous-Tertiary thermotectonic history of the Apuseni Mountains. *Tectonics*, 30(6): TC6008.

Niu, Y., Liu, Y., Xue, Q., Shao, F., Chen, S., Duan, M., Guo, P., Gong, H., Hu, Y., Hu, Z., Kong, J., Li, J., Liu, J., Sun, P., Sun, W., Ye, L., Xiao, Y., and Zhang, Y., 2015. Exotic origin of the

Chinese continental shelf: new insights into the tectonic evolution of the western Pacific and eastern China since the Mesozoic. *Science Bulletin*, 60(18): 1598–1616.

Qi Kai, Ren Zhanli, Cui Junping, Yu Qiang, Cao Zhanpeng, Yang Peng, Deng Yaren and Zhang Mengting, 2017. The Meso-Cenozoic Tectonic Thermal Evolution of the Qishan-Linyou Areas in Weibei Uplift of Ordos Basin and Its Response in Geology: Evidence from Fission-track Analysis. *Acta Geologica Sinica*, 91(1): 161–162 (in Chinese with English abstract).

Ren Zhanli, Cui Junping, Guo Ke, Tian Tao, Li Hai, Wang Wei, Yang Peng and Cao Zhanpeng, 2015. Fission-track analysis of uplift times and processes of the Weibei Uplift in the Ordos Basin. *Chinese Science Bulletin* (Chinese Version), 60(14): 1298–1309 (in Chinese with English abstract).

Ring, U., and Bernet, M., 2010. Fission-track analysis unravels the denudation history of the Bonar Range in the footwall of the Alpine Fault, South Island, New Zealand. *Geological Magazine*, 147(6): 801–813.

Ritts, B.D., Weislogel, A., Graham, S.A., and Darby, B.J., 2009. Mesozoic Tectonics and Sedimentation of the Giant Polyphase Nonmarine Intraplate Ordos Basin, Western North China Block. *International Geology Review*, 51(2): 95–115.

Savignano, E., Mazzoli, S., Arce, M., Franchini, M., Gautheron, C., Paolini, M., and Zattin, M., 2016. (Un)Coupled thrust belt-foreland deformation in the northern Patagonian Andes: New insights from the Esquel-Gastre sector (41° 30′–43° S). *Tectonics*, 35(11): 2636–2656.

Sueoka, S., Shimada, K., Ishimaru, T., Niwa, M., Yasue, K., Umeda, K., Danhara, T., and Iwano, H., 2017. Fission track dating of faulting events accommodating plastic deformation of biotites. *Journal of Geophysical Research: Solid Earth*, 122 (3): 1848–1859.

Tagami, T., 2005. Zircon Fission-Track Thermochronology and Applications to Fault Studies. *Reviews in Mineralogy and Geochemistry*, 58(1): 95–122.

Tagami, T., 2012. Thermochronological investigation of fault zones. *Tectonophysics*, 538–540: 67–85.

Tang Xiyuan, Guo Zhongming, Chen Heli, Wang Runsan, Li Duxing and Zhang Jun, 1992. *Thrust nappe structure and its oil and gas exploration in western margins of Ordos Basin*. Xi'an: Northwest University Press, 143 (in Chinese).

Tian, Y., Qiu, N., Kohn, B.P., Zhu, C., Hu, S., Gleadow, A.J.W., and McInnes, B.I.A., 2012. Detrital zircon (U–Th)/He thermochronometry of the Mesozoic Daba Shan Foreland Basin, central China: Evidence for timing of post-orogenic denudation. *Tectonophysics*, 570–571: 65–77.

Tremblay, A., Roden-Tice, M.K., Brandt, J.A., and Megan, T.W., 2013. Mesozoic fault reactivation along the St. Lawrence rift system, eastern Canada: Thermochronologic evidence from apatite fission-track dating. *Geological Society of America Bulletin*, 125(5–6): 794–810.

Vermeesch, P., and Tian, Y., 2014. Thermal history modelling: HeFTy vs. QTQt. *Earth-Science Reviews*, 139: 279–290.

Wang Jianqiang, Liu Chiyang, Gao Fei, Zhang Dongdong, Li Yongxiang and Li Zhichao, 2015. Pre-Cenozoic geological characteristics and oil-gas significance in Weihe basin, Shaanxi Province. *Geological Bulletin of China*, 34(10): 1981–1991 (in Chinese with English abstract).

Wang Jianqiang, Liu Chiyang, Yan Jianping, Zhao Hongge, Gao Fei and Liu Chao, 2010. Development time and evolution characteristics of Weibei uplift in the south of Ordos basin. *Journal of Lanzhou University* (Natural Sciences), 46(4): 22–29 (in Chinese with English abstract).

Wang, F., Zhu, R., Hou, Q., Zheng, D., Yang, L., Wu, L., Shi, W., Feng, H., Sang, H., Zhang, H. and Liu, Q., 2014. $^{40}Ar/^{39}Ar$ Thermochronology on Central China Orogen: Cooling, uplift and implications for orogeny dynamics. *Geological Society, London, Special Publications*, 378: 189–206.

West Jr, D. P., and Roden-Tice, M. K., 2003. Late Cretaceous reactivation of the Norumbega fault zone, Maine: Evidence from apatite fission-track ages. *Geology*, 31(7): 649–652.

Witt, C., Brichau, S., and Carter, A., 2012. New constraints on the origin of the Sierra Madre de Chiapas (south Mexico) from sediment provenance and apatite thermochronometry. *Tectonics*, 31(6): TC6001.

Xiao Hui, Li Jianxin, Han Wei and Yang Qiongjing, 2013. The tectonic uplift time and evolution characteristics of Weibei uplift in the south edge of Ordos Basin. *Journal of Xi'an University of Science and Technology*, 33(5): 576–582 (in Chinese with English abstract).

Yang Chenyi, 2015. *The Research about Activity of Kouzhen-Guanshan Fault in the North of Weihe Basin*. Xi'an: Northwest University (Master's Thesis): 1–68 (in Chinese with English abstract).

Yang Minghui, Li Liang, Zhou Jin, Jia Huichong, Sun Xiao, Gong Ting and Ding Chao, 2015. Structural evolution and hydrocarbon potential of the upper Paleozoic northern Ordos basin, north China. *Acta Geologica Sinica* (English Edition), 89(5): 1636–1648.

Yang, M., Li, L., Zhou, J., Jia, H., Sun, X., Qu, X., Zhou, D., Gong, T., and Ding, C., 2015. Mesozoic structural evolution of the Hangjinqi area in the northern Ordos Basin, North China. *Marine and Petroleum Geology*, 66: 695–710.

Yang, Y., Li, W., and Ma, L. 2005. Tectonic and stratigraphic controls of hydrocarbon systems in the Ordos basin: A multicycle cratonic basin in central China. *AAPG Bulletin*, 89 (2): 255–269.

Yang, Z., Shen, C., Ratschbacher, L., Enkelmann, E., Jonckheere, R., Wauschkuhn, B., and Dong, Y., 2017. Sichuan Basin and beyond: Eastward foreland growth of the Tibetan Plateau from an integration of Late Cretaceous-Cenozoic fission track and (U-Th)/He ages of the eastern Tibetan Plateau, Qinling, and Daba Shan. *Journal of Geophysical Research: Solid Earth*, 122(6): 4712–4740.

Yin, A., and Nie, S., 1996. A Phanerozoic palinspastic reconstruction of China and its neighboring region. In: Yin, A. and Harrison, T.M. (eds.), *The Tectonic Evolution of Asia*. New York: Cambridge University, 442–485.

Zhai Mingguo, 2011. Cratonization and the Ancient North China Continent: A summary and review. *Science China Earth Sciences*, 54(8): 1110–1120.

Zhai, M., Hu, B., Zhao, T., Peng, P., and Meng, Q., 2015. Late Paleoproterozoic–Neoproterozoic multi-rifting events in the North China Craton and their geological significance: A study advance and review. *Tectonophysics*, 662: 153–166.

Zhang Beihang, Zhang Jin, Wang Yannan, Zhao Heng and Li Yanfeng, 2017. Late Mesozoic–Cenozoic Exhumation of the Northern Hexi Corridor: Constrained by Apatite Fission Track Ages of the Longshoushan. *Acta Geologica Sinica* (English Edition), 91(5): 1624–1643.

Zhang Yueqiao, Shi Wei and Dong Shuwen, 2011. Changes of

Late Mesozoic Tectonic Regimes around the Ordos Basin (North China) and their Geodynamic Implications. *Acta Geologica Sinica* (English Edition), 85(6): 1254–1276.

Zhao Junfeng, Liu Chiyang, Wang Xiaomei and Zhang Can, 2009. Migration of Depocenters and Accumulation Centers and its Indication of Subsidence Centers in the Mesozoic Ordos Basin. *Acta Geologica Sinica* (English Edition), 83(2): 278–294.

Zhao Xiaochen, Liu Chiyang, Wang Jianqiang, Zhao Yan, Zhang Dongdong, Wang Lei, Deng Yu and Guo Pei, 2016. Mesozoic –Cenozoic tectonic uplift events of Xiangshan Mountain in northern North-South Tectonic Belt, China. *Acta Petrologica Sinica*, 32(7): 2124–2136 (in Chinese with English abstract).

Zheng, D., Zhang, P.-Z., Wan, J., Yuan, D., Li, C., Yin, G., Zhang, G., Wang, Z., Min, W., and Chen, J., 2006. Rapid exhumation at ~8 Ma on the Liupan Shan thrust fault from apatite fission-track thermochronology: Implications for growth of the northeastern Tibetan Plateau margin. *Earth and Planetary Science Letters*, 248(1–2): 198–208.

Zhou Dingwu, Li Wenhou, Zhang Yunxiang, Zhang Chengli, Zhang Fuxin, Liu Yiqun, Fu Junhui and Yue Leping, 2002. *The ways and means, practica of the overall research on regional geology*. Beijing: Science Press, 347 (in Chinese with English abstract).

About the first author

ZHANG Shaohua, male, born in 1990 in Baoji City, Shaanxi Province. He is now a Ph.D. candidate of Northwest University. His current research interests include basin analysis, regional tectonics, and petroleum geology. E-mail: zhangshh86@163.com.